Investigation of multistep effects for proton inelastic scattering to the 2_1^+ state in ^{6}He

Shoya Ogawa,[1,*] Takuma Matsumoto,[1,†] Yoshiko Kanada-En'yo,[2,‡] and Kazuyuki Ogata[3,4,5,§]

[1]*Department of Physics, Kyushu University, Fukuoka 819-0395, Japan*
[2]*Department of Physics, Kyoto University, Kyoto 606-8502, Japan*
[3]*Research Center for Nuclear Physics (RCNP), Osaka University, Ibaraki 567-0047, Japan*
[4]*Department of Physics, Osaka City University, Osaka 558-8585, Japan*
[5]*Nambu Yoichiro Institute of Theoretical and Experimental Physics (NITEP), Osaka City University, Osaka 558-8585, Japan*

(Received 31 March 2021; accepted 24 September 2021; published 11 October 2021)

Multistep effects among bound, resonant, and nonresonant states have been investigated by the continuum-discretized coupled-channels method (CDCC). In the CDCC, a resonant state is treated as multiple states fragmented in a resonance energy region, although it is described as a single state in usual coupled-channels calculations. For such the fragmented resonant states, one-step, and multistep contributions to the cross sections should be carefully discussed because the cross sections obtained by the one-step calculation depend on the number of those states, which corresponds to the size of the model space. To clarify the role of the multistep effects, we propose the one-step calculation without model-space dependence for the fragmented resonant states. Furthermore, we also discuss the multistep effects among the ground, 2_1^+ resonant, and nonresonant states in ^{6}He for proton inelastic scattering.

DOI: 10.1103/PhysRevC.104.044608

I. INTRODUCTION

Resonances are metastable states that appear beyond the particle decay threshold in numerous quantum systems. In nuclei, there exist various resonances, such as single-particle resonances, giant resonances, and cluster resonances, that reflect various nucleon correlations. The investigation of such resonances has attracted substantial attention. Recently, resonances of nuclei near or beyond the neutron drip line have been investigated through radioactive ion-beam experiments [1–5]. To elucidate the properties of resonances, their transition cross sections can be experimentally measured via inelastic scattering and/or transfer reactions. Therefore, it is highly desirable to analyze the experimental data by precise theoretical calculations to extract the properties of resonances.

Coupled-channels (CC) calculations provide a reliable method to describe the transition to excited bound and resonant states and have been successfully applied to the analysis of various reactions [6–12]. In CC calculations, higher-order coupling effects between the states considered in the scattering are included. As an alternative to CC calculations, approximate calculations considering only the one-step process have been frequently applied to the analysis of inelastic scattering [4,13–17]. These approximations are referred to as one-step calculations, and the difference between the results of CC and one-step calculations represents the multistep effects. At intermediate and high incident energies, the multistep effects become small and one-step calculations work well, in general.

Recently, proton inelastic scattering to the 2_1^+ state of ^{6}He at 41 MeV/nucleon [13] was analyzed by two methods, namely, the microscopic CC method based on antisymmetrized molecular dynamics (AMD) [18], which is referred to as AMD-MCC, and the continuum-discretized coupled-channels method (CDCC) [19]. In the AMD-MCC, the 2_1^+ state is represented by a bound-state approximation, whereas the coupling potential between the ground and the 2_1^+ states in ^{6}He is calculated by the microscopic folding model with the Melbourne g matrix [13,14,20–26]. The AMD-MCC has been successfully applied to the analysis of various cases of inelastic scattering [9–12,18,27–31]. On the other hand, the CDCC takes into account coupling effects to not only the 2_1^+ state but also the nonresonant states, which are represented by a finite number of discretized states. The CDCC has also been successfully used to describe reactions involving unstable nuclei [32–35]. Thus, although both methods reproduce the inelastic data reasonably well, they afford different views of the multistep effects for the 2_1^+ state.

In the AMD-MCC, the inelastic cross section obtained from the CC calculations is in good agreement with that derived from one-step calculations. This result demonstrates that the multistep effects between the ground and the 2_1^+ states are small. On the other hand, the cross section obtained from the CDCC is not consistent with that provided by the one-step calculations, indicating that the multistep effects make a significant contribution to the inelastic cross section.

One of reasons for this discrepancy concerning the significance of multistep effects is considered to be the influence of nonresonant states, which are taken into account in the CDCC but not in the AMD-MCC. In addition, the resonant

*s-ogawa@phys.kyushu-u.ac.jp
†matsumoto@phys.kyushu-u.ac.jp
‡yenyo@ruby.scphys.kyoto-u.ac.jp
§kazuyuki@rcnp.osaka-u.ac.jp

state is fragmented into multiple states in the CDCC. The one-step calculation in the CDCC neglects the multistep effects between the fragmented resonant states, which are significant because the resonant state can be regarded as a single state. Furthermore it is known that the cross sections to the fragmented states in the one-step calculations are dependent on the number of these states, which corresponds to the size of the model space. To clarify the coupling effects to the nonresonant states, detailed examination of the treatment of the fragmented resonant states is required.

In this paper, we examine the contributions of fragmented resonant states to the inelastic cross section and attempt to clarify the multistep effects between the ground and the resonant states. To this end, we propose a new treatment for the fragmented states without the model-space dependence. To confirm the validity of this approach, we first analyze the three-body reaction of the ^{6}Li + ^{40}Ca system, where ^{6}Li is described as a $d + \alpha$ two-body system because it is easy to adjust the size of the model space. Finally, we discuss the multistep effects in the proton inelastic scattering of ^{6}He.

This paper is organized as follows. In Sec. II, we describe the theoretical framework. In Sec. III, we present and discuss the numerical results. Finally, in Sec. IV, we provide a summary of the key findings.

II. FORMALISM

In the present paper, we consider a projectile breakup reaction in which the projectile has one bound state and one resonant state. In the CDCC, the reaction is assumed to take place in a model space $\mathcal{P}$ defined by

$$\mathcal{P} = |\Phi_0\rangle\langle\Phi_0| + \sum_{\gamma=1}^{N} |\Phi_\gamma\rangle\langle\Phi_\gamma| \equiv \mathcal{P}_0 + \sum_{\gamma} \mathcal{P}_\gamma, \quad (1)$$

where Φ_0 and Φ_γ are the wave functions of the ground state and the discretized continuum states with quantum number γ, respectively. $\mathcal{P}_0$ and $\mathcal{P}_\gamma$ are projection operators on Φ_0 and Φ_γ, respectively. It should be noted here that Φ_γ includes the fragmented resonant states. In the present analysis, we adopt the pseudostate discretization with the Gaussian expansion method to obtain a set of $\{\Phi_\gamma\}$.

In the space $\mathcal{P}$, the Schrödinger equation for the scattering can be expressed as

$$\mathcal{P}(K + U + h - E)\mathcal{P}\Psi = 0, \quad (2)$$

where K and U denote the kinetic energy and potential between the projectile and the target, respectively. The internal Hamiltonian of the projectile h satisfies

$$\varepsilon_0 = \langle\Phi_0|h|\Phi_0\rangle, \quad \varepsilon_\gamma = \langle\Phi_\gamma|h|\Phi_\gamma\rangle. \quad (3)$$

Multiplying $\mathcal{P}_0$ and $\mathcal{P}_\gamma$ from the left side in Eq. (2) leads to the CDCC equation,

$$[K + \mathcal{P}_0 U \mathcal{P}_0 - (E - \varepsilon_0)]\mathcal{P}_0\Psi = -\sum_{\gamma'\neq 0} \mathcal{P}_0 U \mathcal{P}_{\gamma'}\Psi,$$
$$[K + \mathcal{P}_\gamma U \mathcal{P}_\gamma - (E - \varepsilon_\gamma)]\mathcal{P}_\gamma\Psi = -\sum_{\gamma'\neq\gamma} \mathcal{P}_\gamma U \mathcal{P}_{\gamma'}\Psi. \quad (4)$$

In the CDCC, $\mathcal{P}_0\Psi$ and $\mathcal{P}_\gamma\Psi$ can be solved under appropriate boundary conditions, the details of which can be found in Ref. [32].

In contrast to Eq. (5) of the CDCC calculation, the equation of the one-step calculation is given as

$$[K + \mathcal{P}_0 U \mathcal{P}_0 - (E - \varepsilon_0)]\mathcal{P}_0\Psi = 0,$$
$$[K + \mathcal{P}_\gamma U \mathcal{P}_\gamma - (E - \varepsilon_\gamma)]\mathcal{P}_\gamma\Psi = -\mathcal{P}_\gamma U \mathcal{P}_0\Psi. \quad (5)$$

The first line of Eq. (5) is not a coupling equation, and coupling effects from other states are neglected. In the second line of Eq. (5), only the one-step coupling effect from $\mathcal{P}_0\Psi$ is taken into account. It should be noted that the coupling effects between fragmented resonant states are also neglected in Eq. (5).

In the CDCC, we assume that the resonant model space $\mathcal{P}_\mathrm{R}$ can be described by the sum of the fragmented resonant states as

$$\mathcal{P}_\mathrm{R} \equiv \sum_{\gamma_\mathrm{R}} |\Phi_{\gamma_\mathrm{R}}\rangle\langle\Phi_{\gamma_\mathrm{R}}| \equiv \sum_{\gamma_\mathrm{R}} \mathcal{P}_{\gamma_\mathrm{R}}, \quad (6)$$

where γ_R means the quantum number of the fragmented resonant state in γ. Considering the one-step transition to $\mathcal{P}_\mathrm{R}$, the equation to be solved is represented as

$$[K + \mathcal{P}_\mathrm{R} U \mathcal{P}_\mathrm{R} - (E - h)]\mathcal{P}_\mathrm{R}\Psi = -\mathcal{P}_\mathrm{R} U \mathcal{P}_0\Psi. \quad (7)$$

Multiplying $\mathcal{P}_{\gamma_\mathrm{R}}$ from the left-hand side of Eq. (7), the coupling equation for $\mathcal{P}_{\gamma_\mathrm{R}}$ is obtained as

$$\left[K + \mathcal{P}_{\gamma_\mathrm{R}} U \mathcal{P}_{\gamma_\mathrm{R}} - \left(E - \varepsilon_{\gamma_\mathrm{R}}\right)\right]\mathcal{P}_{\gamma_\mathrm{R}}\Psi$$
$$= -\mathcal{P}_{\gamma_\mathrm{R}} U \mathcal{P}_0\Psi - \sum_{\gamma'_\mathrm{R}\neq\gamma_\mathrm{R}} \mathcal{P}_{\gamma_\mathrm{R}} U \mathcal{P}_{\gamma'_\mathrm{R}}\Psi. \quad (8)$$

In Eq. (8), one can see that only coupling effects between the fragmented resonant states are taken into account. In this paper, calculations with Eqs. (5) and (8) are referred to as the *conventional one-step calculation* and *resonant one-step calculation*, respectively. It should be noted here that the discretization of the resonant state does not affect the CDCC equation of Eq. (5).

In practice, we cannot define $\mathcal{P}_\mathrm{R}$ exactly in the CDCC calculation because the fragmented resonant states include not only the resonant component, but also nonresonant components. Thus, we select the fragmented resonant states by determining the energy range in the breakup cross section as described in Sec. III. In the present analysis, the inelastic cross section describing the transition from the ground state to the resonant state is defined by

$$\frac{d\sigma_\mathrm{inel.}}{d\Omega} = \sum_{\gamma_\mathrm{R}} \frac{d\sigma_{\gamma_\mathrm{R}}}{d\Omega}, \quad (9)$$

where $d\sigma_{\gamma_\mathrm{R}}/d\Omega$ represents the cross sections to the fragmented resonant states.

III. RESULTS AND DISCUSSION

A. ^{6}Li scattering

First, we investigate the model-space dependence of the one-step calculation through the analysis of a case of

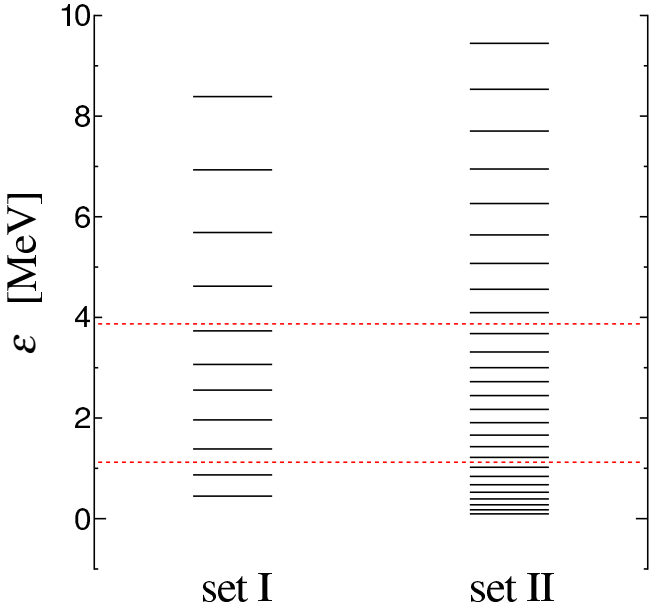

FIG. 1. Pseudostates of ^{6}Li for $I^\pi = 2^+$ calculated with sets I and II. On the vertical axis, 0 MeV corresponds to the $d + \alpha$ threshold. States in the area between the two lines represent fragmented resonant states.

three-body scattering, in which the projectile is described by a two-body model. To this end, we analyze the ^{6}Li + ^{40}Ca reaction at $E = 26$ MeV/nucleon, which was reported in Ref. [36]. The scattering is described by the $d + \alpha + ^{40}$Ca three-body model. The model Hamiltonian H is the same as that used in Ref. [36]. In this model, the spin of the deuteron in ^{6}Li is neglected, the ground state of ^{6}Li has the total spin-parity $I^\pi = 0^+$, and there is one resonant state in $I^\pi = 2^+$. The resonant energy and decay width are 2.75 and 0.2 MeV, respectively.

To study the model-space dependence, we prepare two sets of the discretized states for $I^\pi = 2^+$ of ^{6}Li as set I and set II. The number of discretized states in set II is larger than that in set I as shown in Fig. 1. Here, set I is calculated with the same parameters as in Ref. [36] and gives good convergence of the CDCC. In the pseudostate discretization, the resonant and nonresonant components of a two-body structure can be rather clearly distinguished because the breakup cross sections to discretized states calculated with set I smoothly change with the internal energy of ^{6}Li as shown by histograms in Fig. 2. As the fragmented resonant states, we select states within the range of 1.1 MeV $\leqslant \varepsilon \leqslant$ 3.9 MeV, which corresponds to the region between the two dashed lines in Fig. 1. To clarify the validity of the selection, we calculate the breakup cross section as a function of the internal energy ε of ^{6}Li. In the CDCC, the breakup cross section is described as

$$\frac{d\sigma}{d\varepsilon} = \left| \sum_\gamma f_\gamma(\varepsilon) T_\gamma \right|^2 . \tag{10}$$

T_γ is a discretized T matrix obtained by the CDCC. The histogram values describe $\sigma_\gamma = |T_\gamma|^2$. $f_\gamma(\varepsilon)$ represents the smoothing function, and the details can be found in Ref. [36].

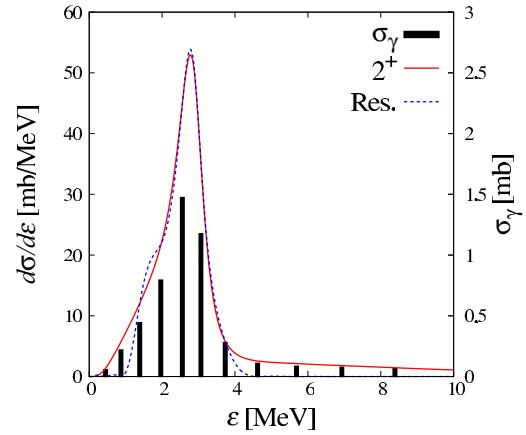

FIG. 2. Breakup cross section for ^{6}Li + ^{40}Ca scattering calculated with set I. The bars represent the breakup cross sections to discretized states, and the absolute values are shown on the right vertical axis.

In Fig. 2, the solid line shows the calculated breakup cross section to $I^\pi = 2^+$ continuum states with set I where all discretized states are taken in the summation of Eq. (10). Meanwhile, the dotted line represents the result taking only the fragmented resonant states. One can see that the solid line is in good agreement with the dotted line around the resonance energy. In the case of set II, we performed the same analysis and found that the energy range is the same as one of set I. Thus, we conclude that the states within the range of 1.1 MeV $\leqslant \varepsilon \leqslant$ 3.9 MeV correspond to the fragmented resonant states. The number of the fragmented resonant states in set I (set II) is five (ten). We discuss the behavior of the wave functions of discretized states in the Appendix.

In Fig. 3, we show the inelastic cross sections to the fragmented resonant 2^+_1 states calculated by the CDCC using

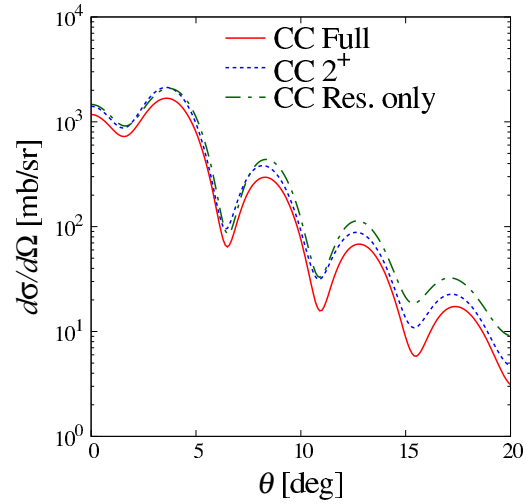

FIG. 3. Inelastic cross sections for the ^{6}Li + ^{40}Ca reaction at $E = 26$ MeV/nucleon obtained from the CDCC. The pseudostates considered in the results are calculated with parameter set I for Gaussian bases.

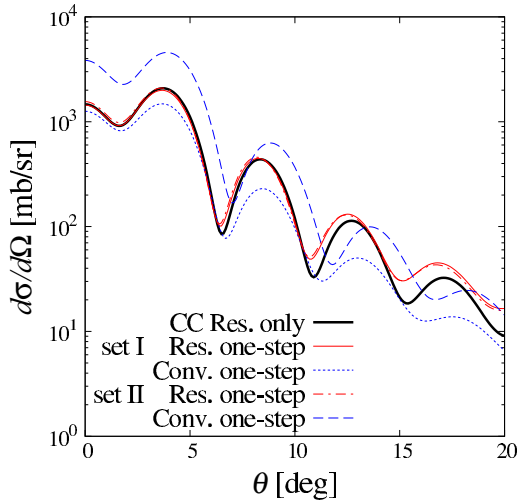

FIG. 4. Inelastic cross sections for the ^{6}Li + ^{40}Ca reaction at $E = 26$ MeV/nucleon obtained from the one-step calculations with Eqs. (5) and (8). The pseudostates considered in the results are calculated with parameter sets I or II for Gaussian bases.

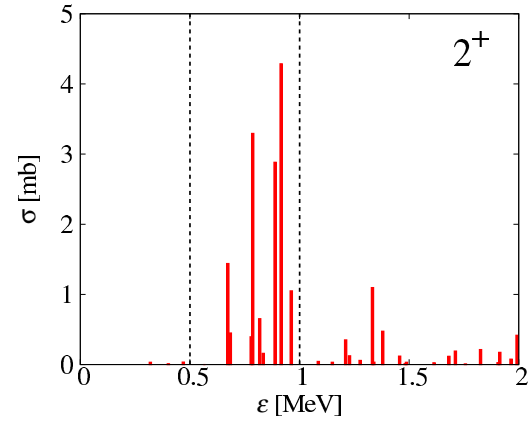

FIG. 5. Breakup cross section for the ^{6}He + p reaction at $E = 41$ MeV/nucleon describing the transition to the 2^+ continuum states obtained from the CDCC. States in the area between the two lines represent fragmented resonant states.

Eq. (9) with set I. It should be noted that if set II is used in the calculations, we obtain the same results. The solid line shows the result of the CDCC with coupling effects of all states for $I^\pi = 0^+$ and 2^+. The dotted and dot-dashed lines indicate the results of the CDCC with all 2^+ states including nonresonant states and only the fragmented resonant states, respectively. The difference between the solid and the dotted lines represents the coupling effects for $I^\pi = 0^+$, and it reduces the cross section by approximately 20–30%. In contrast, the difference between the dotted and the dot-dashed lines, which corresponds to the coupling effects of nonresonant states in $I^\pi = 2^+$, is negligible.

In Fig. 4, we consider the model-space dependence by comparing the inelastic cross sections obtained from the conventional and resonant one-step calculations. The thick solid line denotes the result of the CDCC with only fragmented resonant states for set I, which is the same as the dot-dashed line in Fig. 3. The thin solid and dotted lines represent the results obtained for set I from the conventional and resonant one-step calculations, respectively. The difference between the two results originates from coupling effects between fragmented resonant states. The dot-dashed and dashed lines show the results obtained for set II. One can see that the result of the resonant one-step calculation for set I is in good agreement with that for set II. Furthermore, the result of the resonant one-step calculation is also consistent with that of the CDCC with only fragmented resonant states. This means that the multistep effects between the ground and the resonant states are negligible. On the other hand, the results obtained from the conventional one-step calculation vary with the model space with substantially higher values for set II. This problem is considered to originate from the omission of coupling effects between the fragmented resonant states in the conventional one-step calculations. Thus, we conclude that the resonant one-step calculation should be adopted to estimate the multistep effects for the resonant state in a manner that is independent of the size of the model space in the CDCC framework.

B. ^{6}He scattering

Finally, we discuss the multistep effects in the ^{6}He + p reactions at $E = 41$ and 25 MeV/nucleon in which ^{6}He is described by the ^{4}He $+n + n$ three-body model. In this analysis, we use the same model parameters as described in Ref. [19]. The resonant energy and decay width of the 2^+_1 state are 0.848 and 0.136 MeV, respectively. In contrast to the two-body model of ^{6}Li, the discretized breakup cross sections in the three-body model of ^{6}He exhibit no regularity with respect to the internal energy of ^{6}He as shown in Fig. 5. Therefore, it is not easy to identify the fragmented resonant states. In the present calculations, we select states within the range of $0.5\ \text{MeV} \leqslant \varepsilon \leqslant 1.0\ \text{MeV}$ as the fragmented resonant states for simplicity. The number of the fragmented states is ten. Recently, a new method has been proposed for characterizing resonant states out of pseudostates obtained by diagonalizing a three-body Hamiltonian [37]. Application of this technique to the present paper will be interesting and an important future work.

In Fig. 6, we show the inelastic cross sections to the fragmented resonant 2^+_1 states calculated using Eq. (9). It should be noted that the dashed line is consistent with the cross section to the 2^+_1 state calculated with the complex-scaling method shown in Fig. 3 in Ref. [19]. The solid and dot-dashed lines indicate the results of the resonant one-step calculation and the CDCC with only the fragmented resonant states, respectively. One can see that the solid line is in good agreement with the dot-dashed line. This indicates that the multistep effects between the ground state and the 2^+_1 state are negligible, which is consistent with the results of the AMD-MCC reported in Ref. [18]. On the other hand, the value from the conventional one-step calculation shown by the dotted line is larger than one from the resonant one-step calculation at backward angles, and it looks like the multistep effects are much significant. However, the result of the conventional one-step

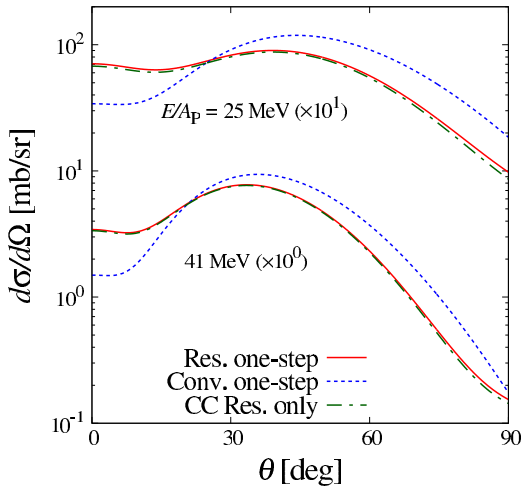

FIG. 6. Inelastic cross sections for the ^{6}He + p reaction at E = 41 and 25 MeV/nucleon obtained from the CDCC including only the fragmented resonant states and one-step calculations using Eqs. (5) and (8).

calculation depends on the size of three-body (^{4}He $+n+n$) model space as mentioned above, and the difference between the dotted and the dot-dashed lines no longer indicates the multistep effects. We, thus, conclude that the multistep effects between the ground state and the 2^+_1 state shown by the difference between the solid and the dot-dashed lines are negligible.

Furthermore, we discussed the coupling effects on the resonant state in Fig. 7. The solid line indicates the result of the resonant one-step calculation. The dotted (dot-dashed) line represents the result of the CDCC with coupling between only $I^\pi = 0^+(0^+, 1^-)$ nonresonant states and the fragmented resonant states. The dashed line corresponds to the result of the CDCC with coupling between all states in the model space. It is found that the cross sections decrease as the coupling effects on the nonresonant states are taken. These effects reduce the

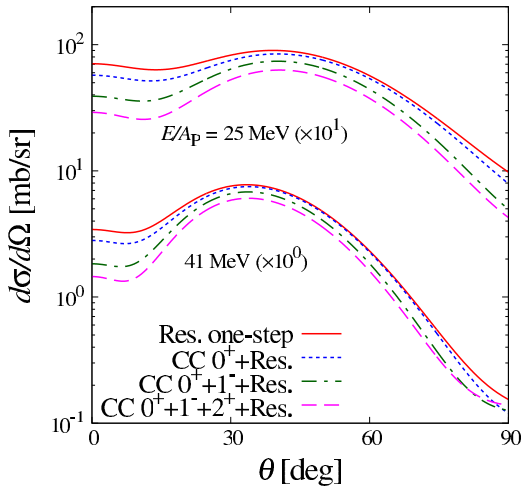

FIG. 7. Inelastic cross sections for the ^{6}He + p reaction at E = 41 and 25 MeV/nucleon obtained from the CDCC and one-step calculations using Eq. (8).

cross section by approximately 20–30% at 41 MeV/nucleon and become stronger as the incident energy decreases.

IV. SUMMARY

We have investigated the multistep effects between the ground and the resonant states by comparing the results of CC calculations and one-step calculations. In the CDCC, the resonant state is fragmented into multiple discretized states where the number of fragmented resonant states is dependent on the size of the model space. In this paper, we introduced two approaches for the one-step calculations, which we refer to as conventional one-step calculation and resonant one-step calculation. The former includes no coupling effects between the fragmented resonant states, whereas the latter considers only the multistep effects between the fragmented resonant states.

In the analysis of ^{6}Li + ^{40}Ca scattering, we confirmed the model-space dependence in the conventional and resonant one-step calculations. The numerical results obtained from the conventional one-step calculation did not converge with increasing the size of the model space; in other words, this result was unphysical. In contrast, the results of the resonant one-step calculation were independent of the size of the model space. Therefore, the resonant one-step calculation is suitable for investigating the multistep effects between resonant states and other states. We have also discussed the multistep effects for the resonance 2^+_1 in ^{6}He via the ^{6}He + p reaction. The numerical results demonstrated that the multistep effects between the 2^+_1 and the ground states were negligible in accordance with Ref. [18] in which the resonance 2^+_1 was obtained as a single state. We, thus, conclude that it is reasonable to describe the resonant state as an excited bound state. Meanwhile, the coupling effects to nonresonant states for $I^\pi = 0^+$, 1^-, and 2^+ are important and reduce the cross section by approximately 20–30% at 41 MeV/nucleon and become stronger at 25 MeV/nucleon. This result originates from the fact that ^{6}He is an unstable nucleus. Therefore, analyses of unstable nuclei should take into account the coupling effects to nonresonant states.

ACKNOWLEDGMENTS

This work was supported, in part, by a Grant-in-Aid for Scientific Research (Grants No. JP18K03650, No. 18K03617, and No. 18H05407) from the Japan Society for the Promotion of Science (JSPS).

APPENDIX

In Fig. 8, we show the radial wave-functions u of the fragmented resonant and nonresonant states, which are obtained by diagonalizing the internal Hamiltonian of ^{6}Li in sets I and II. The wave functions are normalized as $\int_0^\infty |u|^2 dr = 1$. As the fragmented resonant states, we select states with $\varepsilon = 3.05$ MeV in set I (left top panel) and 2.99 MeV in set II (left bottom panel), which are near the resonant energy of 2.75 MeV. The states with $\varepsilon = 4.60$ MeV in set I (right top panel) and $\varepsilon = 5.05$ MeV in set II (right bottom panel) correspond

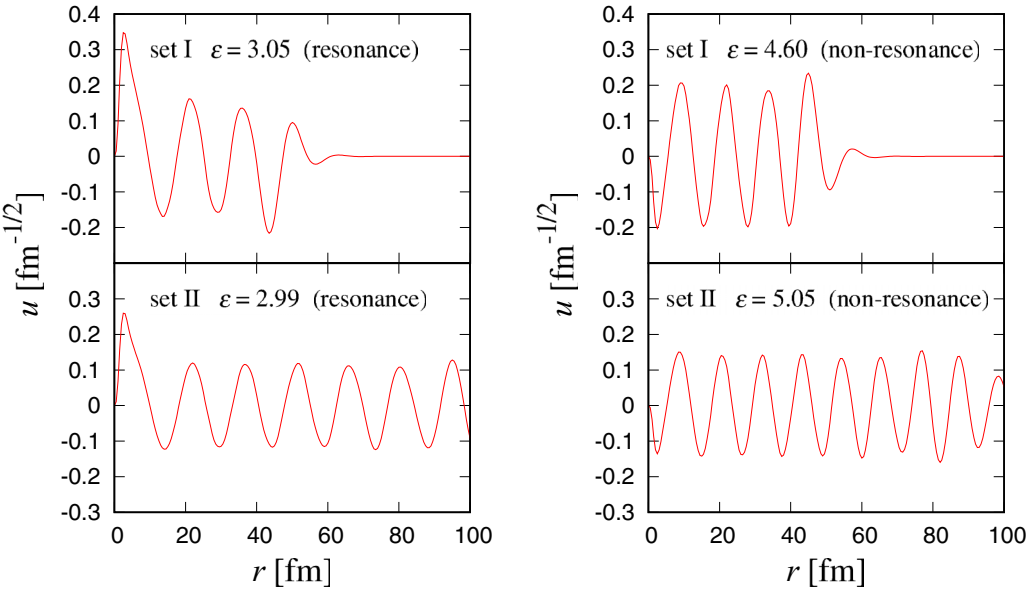

FIG. 8. The radial wave functions of ^{6}Li in sets I and II.

to the nonresonant states. One can see the wave functions in set II oscillate at a longer distance than those in set I because the maximum value of the range parameter $r_{\max}$ in Gaussian bases for sets I and II are taken as 20 and 40 fm, respectively.

Figure 9 shows the radial wave functions in set I. The left and right panels represent the wave functions and the probability densities, respectively. Here we select states with $\varepsilon = 2.54$ MeV (top panel) and 3.05 MeV (midpanel) as the

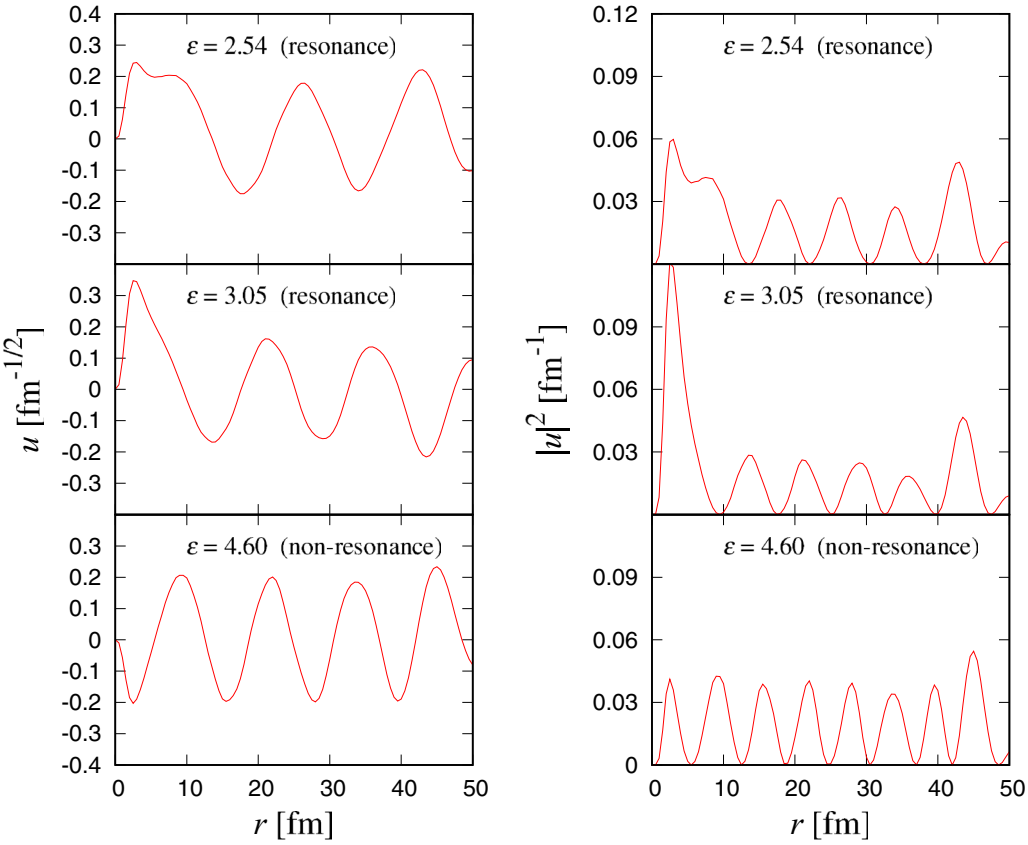

FIG. 9. The radial wave functions of ^{6}Li and the probability densities in set I.

TABLE I. The probabilities obtained of the fragmented resonant and nonresonant states in set I by integrating the probability densities over r up to 20 fm.

	2.54 MeV resonance	3.05 MeV resonance	4.60 MeV nonresonance
Probability	0.532	0.548	0.369

resonant state, and a state with $\varepsilon = 4.60$ MeV (bottom panel) as the nonresonant state. It is found that the fragmented resonant states have large amplitudes in the internal region up to $r_{\max}$. On the other hand, the nonresonant state has a constant amplitude in the whole region. To clear this point, we show the probabilities obtained by integrating the probability densities over r up to $r_{\max}$ in Table I, and the values of the fragmented resonant states are larger than one of the nonresonant state.

[1] A. Spyrou, Z. Kohley, T. Baumann, D. Bazin, B. A. Brown, G. Christian, P. A. DeYoung, J. E. Finck, N. Frank, E. Lunderberg, S. Mosby, W. A. Peters, A. Schiller, J. K. Smith, J. Snyder, M. J. Strongman, M. Thoennessen, and A. Volya, Phys. Rev. Lett. **108**, 102501 (2012).

[2] R. Kanungo, A. Sanetullaev, J. Tanaka, S. Ishimoto, G. Hagen, T. Myo, T. Suzuki, C. Andreoiu, P. Bender, A. A. Chen, B. Davids, J. Fallis, J. P. Fortin, N. Galinski, A. T. Gallant, P. E. Garrett, G. Hackman, B. Hadinia, G. Jansen, M. Keefe *et al.*, Phys. Rev. Lett. **114**, 192502 (2015).

[3] Y. Kondo, T. Nakamura, R. Tanaka, R. Minakata, S. Ogoshi, N. A. Orr, N. L. Achouri, T. Aumann, H. Baba, F. Delaunay, P. Doornenbal, N. Fukuda, J. Gibelin, J. W. Hwang, N. Inabe, T. Isobe, D. Kameda, D. Kanno, S. Kim, N. Kobayashi *et al.*, Phys. Rev. Lett. **116**, 102503 (2016).

[4] J. Tanaka *et al.*, Phys. Lett. B **774**, 268 (2017).

[5] Y. L. Sun *et al.*, Phys. Lett. B **814**, 136072 (2021).

[6] D. T. Khoa and D. C. Cuong, Phys. Lett. B **660**, 331 (2008).

[7] M. Takashina, T. Furumoto, and Y. Sakuragi, Phys. Rev. C **81**, 047605 (2010).

[8] T. Furumoto, T. Suhara, and N. Itagaki, Phys. Rev. C **87**, 064320 (2013).

[9] Y. Kanada-En'yo and K. Ogata, Phys. Rev. C **99**, 064601 (2019).

[10] Y. Kanada-En'yo and K. Ogata, Phys. Rev. C **99**, 064608 (2019).

[11] Y. Kanada-En'yo and K. Ogata, Phys. Rev. C **100**, 064616 (2019).

[12] Y. Kanada-En'yo and K. Ogata, Phys. Rev. C **101**, 064607 (2020).

[13] A. Lagoyannis *et al.*, Phys. Lett. B **518**, 27 (2001).

[14] S. V. Stepantsov *et al.*, Phys. Lett. B **542**, 35 (2002).

[15] D. T. Khoa *et al.*, Nucl. Phys. A **759**, 3 (2005).

[16] H. Al Falou *et al.*, Phys. Lett. B **721**, 224 (2013).

[17] L. R. Gasques, A. S. Freitas, L. C. Chamon, J. R. B. Oliveira, N. H. Medina, V. Scarduelli, E. S. Rossi, Jr., M. A. G. Alvarez, V. A. B. Zagatto, J. Lubian, G. P. A. Nobre, I. Padron, and B. V. Carlson, Phys. Rev. C **97**, 034629 (2018).

[18] Y. Kanada-En'yo and K. Ogata, arXiv:2004.14597.

[19] S. Ogawa and T. Matsumoto, Phys. Rev. C **102**, 021602(R) (2020).

[20] K. Amos *et al.*, in *Advances in Nuclear Physics*, edited by J. W. Negele and E. Vogt (Plenum, New York, 2000), Vol. 25, p. 275.

[21] S. Karataglidis, Y. J. Kim, and K. Amos, Nucl. Phys. A **793**, 40 (2007).

[22] K. Minomo *et al.*, J. Phys. G: Nucl. Part. Phys. **37**, 085011 (2010).

[23] M. Toyokawa, K. Minomo, and M. Yahiro, Phys. Rev. C **88**, 054602 (2013).

[24] K. Egashira, K. Minomo, M. Toyokawa, T. Matsumoto, and M. Yahiro, Phys. Rev. C **89**, 064611 (2014).

[25] K. Minomo and K. Ogata, Phys. Rev. C **93**, 051601(R) (2016).

[26] K. Minomo, K. Washiyama, and K. Ogata, arXiv:1712.10121.

[27] Y. Kanada-En'yo and K. Ogata, Phys. Rev. C **101**, 014317 (2020).

[28] Y. Kanada-En'yo and K. Ogata, Phys. Rev. C **101**, 064308 (2020).

[29] Y. Kanada-En'yo, Y. Shikata, Y. Chiba, and K. Ogata, Phys. Rev. C **102**, 014607 (2020).

[30] Y. Kanada-En'yo and K. Ogata, Phys. Rev. C **103**, 024603 (2021).

[31] Y. Kanada-En'yo and K. Ogata, Prog. Theor. Exp. Phys. **2021**, 043D01 (2021).

[32] M. Yahiro *et al.*, Prog. Theor. Exp. Phys. **2012**, 01A206 (2012).

[33] T. Matsumoto, E. Hiyama, K. Ogata, Y. Iseri, M. Kamimura, S. Chiba, and M. Yahiro, Phys. Rev. C **70**, 061601(R) (2004).

[34] T. Matsumoto, T. Egami, K. Ogata, Y. Iseri, M. Kamimura, and M. Yahiro, Phys. Rev. C **73**, 051602(R) (2006).

[35] T. Matsumoto, J. Tanaka, and K. Ogata, Prog. Theor. Exp. Phys. **2019**, 123D02 (2019).

[36] T. Matsumoto, T. Kamizato, K. Ogata, Y. Iseri, E. Hiyama, M. Kamimura, and M. Yahiro, Phys. Rev. C **68**, 064607 (2003).

[37] J. Casal and J. Gómez-Camacho, Phys. Rev. C **99**, 014604 (2019).